Letter

Order-parameter evolution in the Fulde-Ferrell-Larkin-Ovchinnikov phase

S. Molatta,[1] T. Kotte [1] D. Opherden,[1] G. Koutroulakis,[2,3] J. A. Schlueter,[4,5] G. Zwicknagl [6,7] S. E. Brown,[2] J. Wosnitza,[1,8] and H. Kühne [1,*]

[1]*Hochfeld-Magnetlabor Dresden (HLD-EMFL) and Würzburg-Dresden Cluster of Excellence ct.qmat, Helmholtz-Zentrum Dresden-Rossendorf, 01328 Dresden, Germany*
[2]*Department of Physics and Astronomy, UCLA, Los Angeles, California 90095, USA*
[3]*Department of Physics, UCSB, Santa Barbara, California 93106, USA*
[4]*Materials Science Division, Argonne National Laboratory, Argonne, Illinois 60439, USA*
[5]*Division of Materials Research, National Science Foundation, Alexandria, Virginia 22314, USA*
[6]*Institute for Mathematical Physics, Technische Universität Braunschweig, 38106 Braunschweig, Germany*
[7]*Max Planck Institute for Chemical Physics of Solids, 01187 Dresden, Germany*
[8]*Institut für Festkörper- und Materialphysik, TU Dresden, 01062 Dresden, Germany*

We report on the temperature dependence of the spatially modulated spin-polarization amplitude ΔK_{spin}, which is a hallmark of the superconducting Fulde-Ferrell-Larkin-Ovchinnikov (FFLO) state. For that, we use ^{13}C nuclear magnetic resonance (NMR) spectroscopy performed on the organic conductor β''-(ET)$_2$SF$_5$CH$_2$CF$_2$SO$_3$. From a comparison of our experimental results to a comprehensive modeling of the ^{13}C NMR spectra, we determine the evolution of ΔK_{spin} upon condensation of the FFLO state. Further, the modeling of the spectra in the superconducting phase allows to quantify the decrease of the average spin susceptibility, stemming from the spin-singlet coupling of the superconducting electron pairs in the FFLO state of β''-(ET)$_2$SF$_5$CH$_2$CF$_2$SO$_3$.

Introduction. The Fulde-Ferrell-Larkin-Ovchinnikov (FFLO) state is a superconducting phase of Cooper pairing with nonzero center-of-mass momentum, resulting in a spatial oscillation of the superconducting order parameter. Whereas Fulde and Ferrell as well as Larkin and Ovchinnikov predicted the existence of such a state already in 1964 [1,2], its rigorous experimental verification was achieved only during the last years by means of thermodynamic and spectroscopic methods [3–15]. Although the FFLO state represents a quite general concept of pairing in multicomponent Fermi liquids with strong population imbalance [16,17], clear experimental realizations require stringent conditions, such as an orbital critical field much larger than the Pauli paramagnetic limit, i.e., a Maki parameter $\alpha > 1.8$ [18], and superconductivity in the clean limit with a mean free path much larger than the coherence length [19,20].

This is one of the reasons why it took many years before proven evidence for the existence of FFLO states appeared. In recent years, experimental signatures of FFLO physics have been reported for a number of superconducting materials, such as FeSe [21,22], CeCu$_2$Si$_2$ [23], KFe$_2$As$_2$ [24], CeCoIn$_5$ [25], NbS$_2$ [26], Ba$_6$Nb$_{11}$S$_{28}$ [27], and Sr$_2$RuO$_4$ [28]. However, the clearest evidence for the existence of FFLO states, so far, exists for several quasi-two-dimensional (2D) organic superconductors [3–15]. In particular, various groups reported evidence for an FFLO phase above the Pauli limit of about 9 and 21 T in β''-(ET)$_2$SF$_5$CH$_2$CF$_2$SO$_3$ [with

ET=bis(ethylenedithio)-tetrathiafulvalene] (β''-ET in the following) [3–6] and κ-(ET)$_2$Cu(NCS)$_2$ (κ-ET in the following), respectively [7–15].

Until now, experimental reports of the evolution of the FFLO order parameter upon varying the temperature have been lacking. We may even ask, what actually is the order parameter of the FFLO state and how can it be probed by an experimental observable? At the temperature-driven transition to the FFLO state, the normal state with a finite, homogeneous spin polarization is unstable with respect to the onset of a superconducting order parameter characterized by a modulation at wave vector $\mathbf{Q}$ (FF), or $\mathbf{Q}$ and $-\mathbf{Q}$ (LO). The prior results [6] were interpreted as evidence for a modulated spin polarization, as would be associated with the LO phase. That is, the maximum spin polarization is located at the real-space gap zeros.

Experimentally, it is rather challenging to probe this modulation of the spin polarization. For organic superconductors, magnetic fields of several tesla have to be applied to overcome the Pauli limit, whereas the modulation amplitude is only of the order of a few gauss [6]. Such a resolution is difficult to achieve using scattering or scanning-probe techniques. Nuclear magnetic resonance (NMR) spectroscopy, however, is uniquely suited in this context, as the isotope-specific resonance spectra are a direct measure of the local-field distribution, with very high spectral resolution even at highest magnetic fields. Indeed, NMR experiments of β''-ET and κ-ET showed the emergence of inhomogeneous line broadening in the FFLO regime, which stems from the underlying spatial modulation of the spin polarization [6,9,11].

In the present Letter, we report an experimental study of the emerging inhomogeneous spin-polarization distribution upon condensation of the FFLO state from the normal state in β''-ET by means of ^{13}C NMR spectroscopy. A comprehensive modeling of the spectra allows a quantitative determination of the temperature-dependent spin-modulation amplitude as a probe of the spatially modulated order parameter in the FFLO state. Further, we quantify the decrease of the average local spin susceptibility with temperature, driven by the singlet formation of the superconducting electron pairs in the FFLO state.

Methods. For the experiments, we used a β''-ET single crystal with ^{13}C spin labeling on the central carbon sites of the molecular layers. This crystal, with dimensions of 0.8 mm × 2.5 mm × 0.1 mm, is a piece of the sample investigated in Ref. [6]. We mounted the NMR coil with the sample inside to a mechanical rotator with angular resolution of a few 0.01°, and cooled this setup using a ^{3}He sample-in-liquid top-loading cryostat in a 16-T superconducting magnet with a spatial field homogeneity of 4 ppm over 10 mm. During the experiment, we calibrated the magnetic field repeatedly using the NMR signal of the liquid ^{3}He. We aligned the sample with the magnetic field parallel to the conducting layers within ±0.01°, by probing the rf reflection and the NMR observables as described in Ref. [6]. The ^{13}C NMR spectra were recorded using a top-tuned resonator configuration and via standard Hahn spin-echo detection, with carefully adjusted pulse parameters in order to avoid heating effects. We applied a magnetic field of 10.5 T, somewhat above the Pauli limit of 9.3 T [5], which yields a relatively large modulation amplitude of the superconducting gap and, hence, a large modulation amplitude of the local spin polarization in the FFLO state of β''-ET [6].

Results and discussion. In order to achieve a full understanding of the ^{13}C NMR spectra, we first define the different local-field contributions at the ^{13}C-enriched sites in the molecular layers, as well as the modeling procedure of the corresponding NMR spectra in both the normal-conducting and FFLO state. Finally, we employ the spectral modeling to determine the evolution of the site-specific local spin polarization and modulation amplitude in the FFLO state.

As exemplified in Fig. 1(b), the normal-state spectrum is composed of four line doublets, stemming from the four inequivalent carbon sites at the ^{13}C-labeled central positions in the ET molecules. Two doublets each yield the high- and low-frequency parts of the spectrum, with each part relating to ^{13}C sites in molecular layers of mutually disproportionated charge density, and, thus, site-specific hyperfine coupling to the itinerant charge carriers [29]. Within the high- and low-frequency parts, the two doublets relate to "inner" and "outer" positions of the ^{13}C sites within the molecular layers [30] [compare Fig. 1(a)]. Due to the site-selective spin labeling, the ^{13}C isotopes occur exclusively as neighboring atoms in the molecular structure. The resulting nuclear dipole-dipole interaction leads to the observed doublet structure. Another local-field contribution with site- and molecular-orientation-specific amplitude stems from orbital moments. Lastly, a finite distribution of uniform static local-field components leads to an intrinsic homogeneous line broadening, which scales with the site-dependent hyperfine coupling amplitude.
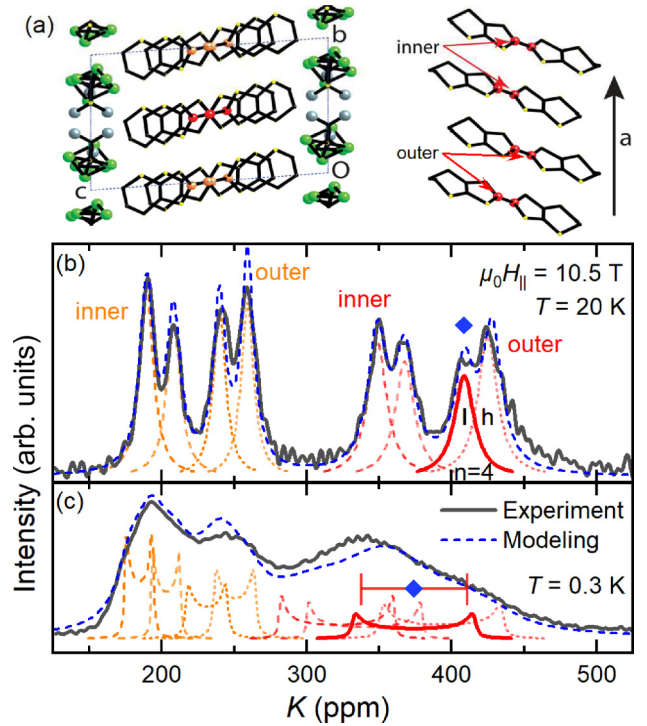

FIG. 1. (a) Crystal structure (left) of β''-ET, projected along the [100] direction. The ET molecules, stacked along [100] and viewed along [010] (right), are ^{13}C labeled on their central positions. (b) and (c) Representative ^{13}C NMR spectra in the normal-conducting and FFLO state, respectively, with the site-resolved contributions to the spectral modeling shown as dashed lines. The modeled spectrum of the line with $n = 4$ and $i = l$ is highlighted by the red bold line, with the site-specific first spectral moment $K_{\text{orb},n=4} + \lambda K_{\text{spin},n=4} - D_{n=4,i=l}$ and the local-polarization modulation $2\lambda K_{\text{spin},n=4} \Delta K_{\text{spin}}$ indicated by the blue diamond and the red horizontal bar, respectively [see Eq. (2)]. In (c), the intrinsic linewidth of the site-specific contributions to the modeled spectrum is minimized to highlight the underlying double-horn shape, resulting from the one-dimensionally modulated spin polarization.

For the modeling of the normal-state spectra, the total shift for each of the eight spectral lines is defined by

$$K_{n,i} = K_{\text{orb},n} + K_{\text{spin},n} \pm D_{n,i}, \qquad (1)$$

where the indices $n = (1, 2, 3, 4)$ and $i = (l, h)$ denote the line doublets and the low- and high-frequency lines within a doublet, respectively. $K_{\text{orb},n}$ and $K_{\text{spin},n}$ are the site-specific orbital and spin-polarization contributions to the shift, respectively, whereas $D_{n,i}$ accounts for the ^{13}C internuclear dipole interaction, thus defining the line splitting and relative intensities within the doublets [31].

In order to extend the modeling formalism to the spectra of the FFLO state, we account for the reduction of the local-spin polarization due to spin-singlet Cooper pairing by normalizing the site-averaged spin part of the Knight shift $\overline{K}_{\text{spin}}$ at a given temperature to that of the normal state, $\overline{K}_{\text{spin,NS}}$, defining the reduction parameter $\lambda = \overline{K}_{\text{spin}}/\overline{K}_{\text{spin,NS}}$. The spatial modulation of the spin polarization in the FFLO state is parametrized by the modulation amplitude ΔK_{spin} and the histogram function $\Gamma(r)$ of the real-space spin modulation,

manifested as inhomogeneous spectral line broadening in the FFLO state.

With these assumptions, the spectral components become a histogram of the site-specific Knight shift according to

$$P(K_{n,i}) = K_{\mathrm{orb},n} + \lambda K_{\mathrm{spin},n}[1 + \Delta K_{\mathrm{spin}}\Gamma(r)] \pm D_{n,i}. \quad (2)$$

Finally, the spectral lines for each of the eight sites are constructed from pseudo-Voigt functions with a dense sampling of $P(K_{n,i})$.

We used Eq. (2) for a consistent modeling of all spectra in the whole temperature range between 0.3 and 20 K. The local-field distribution is consistently described by modeling it as a consequence of a one-dimensional, sinusoidal, spatial modulation [6], i.e., $\Gamma(r) = \sin(2\pi r)$, which is in agreement with the original FFLO prediction [32–35]. The according spectral line resembles a double-horn shape, with the low- and high-frequency horns relating to spatial regions of minimum and maximum local spin polarization, respectively [36].

In order to determine the values of K_{orb}, K_{spin}, and $D_{n,i}$, we first optimized the modeling of the normal-state spectra, i.e., for temperatures between 20 and 2 K, to yield the best global agreement with all experimental spectra in this range. This provided a high numerical stability of the obtained parameters. We show a representative modeled normal-state spectrum and its site-resolved contributions by the dashed lines in Fig. 1(b), yielding a very good agreement with the experimental spectrum at 20 K. We obtain orbital contributions of $K_{\mathrm{orb}} = \{154, 185, 173, 222\}$ ppm at 20 K and normal-state spin contributions of $K_{\mathrm{spin}} = \{45, 65, 185, 196\}$ ppm for the sites $n = 1$–4, respectively, as well as a doublet splitting parameter $D_{n,i}$ of about 9 ppm, with less than 4% variation for the different sites. As expected, the modeling results in $\lambda \approx 1$ and $\Delta K_{\mathrm{spin}} \approx 0$ in the normal-conducting state. The intrinsic linewidth of the pseudo-Voigt functions increases with increasing local spin contribution, and, thus, with increasing hyperfine coupling strength, which correlates this broadening mechanism with a homogeneous distribution of uniform local-field components in the conducting layers.

For the modeling of the spectra in the superconducting state, we kept the values of K_{orb}, K_{spin}, and $D_{n,i}$ fixed. We emphasize that, in order to minimize the number of free parameters, we determined λ and ΔK_{spin} as global parameters per spectrum, i.e., by a simultaneous modeling and summation of the spectral contributions from all four ^{13}C sites. In the FFLO state, λ and ΔK_{spin} yield a temperature-dependent deviation from their normal-state values, reflecting a hyperfine-coupling-dependent and, thus, site-specific inhomogeneous line broadening, as well as a reduction of the first spectral moment, $K_{\mathrm{orb},n} + \lambda K_{\mathrm{spin},n} + D_{n,i}$. A representative modeling of the spectrum at 0.3 K yields a very good agreement with the experimental ^{13}C spectrum, with a site-dependent width of the underlying double-horn shape [Fig. 1(c)].

In order to quantify the spin polarization around the real-space gap zeros, we compare the first moment of the peak with $n = 4$ and $i = l$ at 20 K [Fig. 1(b)] with the higher-frequency horn of the corresponding spectral contribution at 0.3 K [Fig. 1(c)], giving total shift values of $K = 409$ and 411 ppm for 20 and 0.3 K, respectively. This difference is small compared to the normal-state spin polarization $K_{\mathrm{spin}} = 196$ ppm (mentioned above) for this site. Thus, we conclude

that the spin polarization at the real-space gap zeros in the FFLO state is approximately the same as in the normal state.

Figure 2(a) shows the previously reported phase diagram of β''-ET for magnetic fields aligned parallel to the conducting layers, inferred from specific-heat measurements [5]. We performed measurements of ^{13}C NMR spectra at $\mu_0 H_\parallel = 10.5$ T and various temperatures between 0.3 and 20 K, ranging from the normal state far into the FFLO state. Figure 2(b) shows a waterfall diagram of all corresponding experimental spectra. At high temperatures, the spectra yield four line doublets as described above. With lowering temperature, we find a smooth, very weak decrease of the site-specific orbital contributions, with $\Delta K_{\mathrm{orb}}/\Delta T < 1$ ppm/K for all sites, which may be attributed to a small redistribution of charge density in the molecular layers [29]. Below 1.4 K, when entering the FFLO phase, the site-specific shift yields a sudden decrease and inhomogeneous spectral broadening, which is more pronounced for lines with higher shift due to the respective stronger hyperfine coupling. This inhomogeneous line broadening is clear evidence for entering the FFLO state [6].

The modeled spectra, which are color matched to the experimental spectra at the same temperatures, are shown in Fig. 2(c). The modeling yields an excellent reproduction of the experimental spectra for all temperatures, ranging from the normal-conducting state far into the FFLO phase. In particular, below the onset to FFLO superconductivity, the modeling yields a very good reproduction of the temperature-dependent frequency shifts of the different ^{13}C sites, scaling with the respective hyperfine couplings, as well as of the pronounced increase of the inhomogeneous line broadening, stemming from a nonzero ΔK_{spin}.

Finally, Fig. 3 shows the temperature dependence of the reduction parameter λ and the modulation amplitude ΔK_{spin}. The modeling of the NMR spectra yields the emergence of nonzero ΔK_{spin} at $T_c \equiv 1.4$ K as the condensation temperature of a coherent FFLO state, whereas the average spin part of the Knight shift starts to drop below its normal-state value below $T^* \simeq 1.8$ K. This difference might indicate a transition regime governed by pronounced fluctuation effects, before the FFLO lattice becomes static at 1.4 K on the timescale of the NMR spectra, which is of the order of 10 µs. Further investigations of dynamical NMR observables may shed more light on the effects in this regime.

In the FFLO state, the temperature dependence of ΔK_{spin} is indistinguishable from $\Delta K_{\mathrm{spin}} \sim [T_c - T]^{1/2}$, as indicated by the semitransparent red line in Fig. 3. This observation also differs from mean-field expectations [37], although we note that the behavior may be changing very close to the normal-FFLO transition, where our resolution of ΔK_{spin} is limited. Nevertheless, the sharp onset of nonzero ΔK_{spin} is consistent with a continuous normal-FFLO transition in the bulk of the sample. Furthermore, the agreement between measured and modeled ^{13}C NMR spectra clearly indicates a one-dimensional and sinusoidally varying modulation of the spin polarization across the entire range of investigated temperatures. At least at this field strength, and within the accuracy of our results, there are no signs of a transition to a different FFLO-type modulation, which is in agreement with the expectations for the anisotropic Fermi surface of β''-ET. Our results indicate the manifestation of an LO state, with the
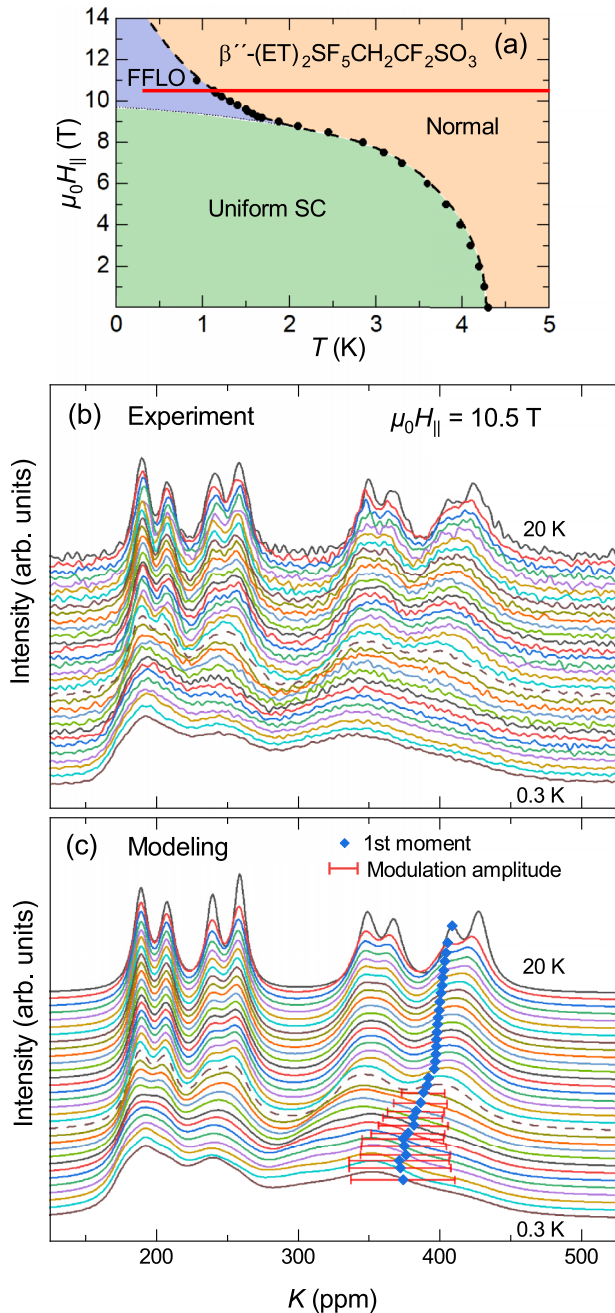
FIG. 2. (a) Superconducting phase diagram of β''-ET for magnetic fields aligned parallel to the conducting layers. The phase boundaries are inferred from specific-heat measurements (black circles) [5], the measurements of ^{13}C NMR spectra at $\mu_0 H_\parallel = 10.5$ T, and various temperatures in this work are indicated by the red horizontal line. (b) Waterfall diagram of the experimental ^{13}C NMR spectra at various temperatures between 0.3 and 20 K (same as the temperatures in Fig. 3). (c) Modeled spectra as described in the main text. Below 1.4 K, indicated by the brown dashed-line spectrum, a decrease of all line shifts is observed, and accompanied by the emergence of inhomogeneous line broadening. As in Fig. 1(c), the spin-polarization modulation amplitude and the first spectral moment of the line with $n = 4$ and $i = l$ are indicated by the red horizontal bar and the blue diamond, respectively.
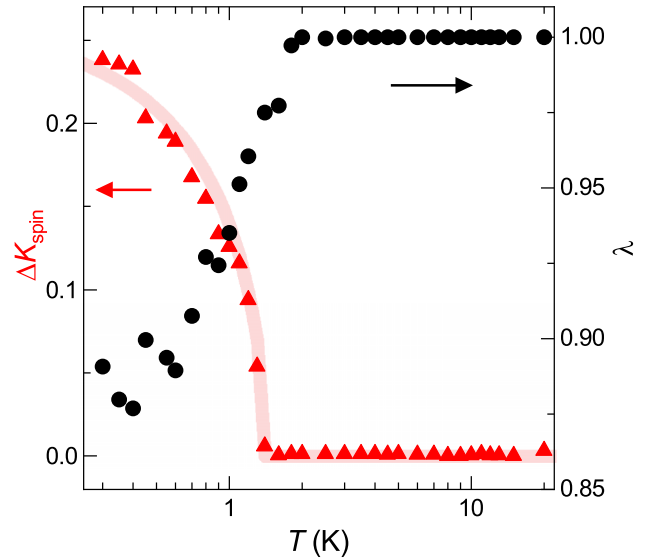

FIG. 3. Temperature dependence of the modulation amplitude ΔK_{spin} (red triangles) and relative reduction λ of the average spin part of the Knight shift (black circles) of β''-ET at $\mu_0 H_\parallel = 10.5$ T.

maximum of the spatially modulated spin polarization being located at the real-space gap zeros. However, the characteristic length scale of the modulation cannot be inferred from the NMR measurements. Rather, the amplitude and dimensionality of the modulation are reflected in the width and shape of the spectral lines [36]. Lastly, we note that impurities do not play a role in the present case, since our NMR results are fully in line with previous results [5].

Conclusion. We have presented an experimental study of the emerging inhomogeneous spin polarization upon condensation of the FFLO state in β''-ET. The modeling of the ^{13}C NMR spectra provides a quantitative description of the spin-modulation amplitude ΔK_{spin} as a probe of the spatially modulated order parameter. Our results show that β''-ET is an excellent material to probe the temperature-driven transition between the normal and the FFLO state, and that allows us to provide a quantitative description of the spin polarization upon condensation of the FFLO state. The implications of our results may be further elucidated by future theoretical work dealing with the spin polarization and FFLO order-parameter evolution upon condensation from the normal state.

Our approach for quantitatively modeling the NMR spectra is independent of the symmetry of the superconducting order parameter. Thus, it would be very interesting to perform similar studies on other FFLO superconductors, such as those mentioned at the beginning of this Letter. However, the feasibility of such studies depends on the availability of very clean samples, which not only feature FFLO superconductivity, but also host a very homogeneous spin susceptibility, on the background of which the very small spin-polarization modulation in the FFLO state can be resolved experimentally. Thus, although the phenomenology of FFLO superconductivity has by now been confirmed by several studies, experimental investigations of the microscopic details in bulk materials remain challenging.

[1] P. Fulde and R. A. Ferrell, Phys. Rev. **135**, A550 (1964).

[2] A. I. Larkin and Y. N. Ovchinnikov, Sov. Phys. JETP **20**, 762 (1965).

[3] S. Sugiura, T. Isono, T. Terashima, S. Yasuzuka, J. A. Schlueter, and S. Uji, npj Quantum Mater. **4**, 7 (2019).

[4] R. Beyer and J. Wosnitza, Low Temp. Phys. **39**, 225 (2013).

[5] R. Beyer, B. Bergk, S. Yasin, J. A. Schlueter, and J. Wosnitza, Phys. Rev. Lett. **109**, 027003 (2012).

[6] G. Koutroulakis, H. Kühne, J. A. Schlueter, J. Wosnitza, and S. E. Brown, Phys. Rev. Lett. **116**, 067003 (2016).

[7] R. Lortz, Y. Wang, A. Demuer, P. H. M. Böttger, B. Bergk, G. Zwicknagl, Y. Nakazawa, and J. Wosnitza, Phys. Rev. Lett. **99**, 187002 (2007).

[8] B. Bergk, A. Demuer, I. Sheikin, Y. Wang, J. Wosnitza, Y. Nakazawa, and R. Lortz, Phys. Rev. B **83**, 064506 (2011).

[9] J. A. Wright, E. Green, P. Kuhns, A. Reyes, J. Brooks, J. Schlueter, R. Kato, H. Yamamoto, M. Kobayashi, and S. E. Brown, Phys. Rev. Lett. **107**, 087002 (2011).

[10] C. C. Agosta, J. Jin, W. A. Coniglio, B. E. Smith, K. Cho, I. Stroe, C. Martin, S. W. Tozer, T. P. Murphy, E. C. Palm, J. A. Schlueter, and M. Kurmoo, Phys. Rev. B **85**, 214514 (2012).

[11] H. Mayaffre, S. Krämer, M. Horvatic, C. Berthier, K. Miyagawa, K. Kanoda, and V. F. Mitrovic, Nat. Phys. **10**, 928 (2014).

[12] S. Tsuchiya, J.-I. Yamada, K. Sugii, D. Graf, J. S. Brooks, T. Terashima, and S. Uji, J. Phys. Soc. Jpn. **84**, 034703 (2015).

[13] C. C. Agosta, N. A. Fortune, S. T. Hannahs, S. Gu, L. Liang, J. H. Park, and J. A. Schleuter, Phys. Rev. Lett. **118**, 267001 (2017).

[14] N. A. Fortune, C. C. Agosta, S. T. Hannahs, and J. A. Schlueter, J. Phys.: Conf. Ser. **969**, 012072 (2018).

[15] T. Kotte, H. Kühne, J. A. Schlueter, G. Zwicknagl, and J. Wosnitza, Phys. Rev. B **106**, L060503 (2022).

[16] G. Zwicknagl and J. Wosnitza, Int. J. Mod. Phys. B **24**, 3915 (2010).

[17] Y. Matsuda and H. Shimahara, J. Phys. Soc. Jpn. **76**, 051005 (2007).

[18] K. Maki and T. Tsuneto, Prog. Theor. Phys. **31**, 945 (1964).

[19] S. Takada, Prog. Theor. Phys. **43**, 27 (1970).

[20] L. W. Gruenberg and L. Gunther, Phys. Rev. Lett. **16**, 996 (1966).

[21] S. Kasahara, Y. Sato, S. Licciardello, M. Čulo, S. Arsenijević, T. Ottenbros, T. Tominaga, J. Böker, I. Eremin, T. Shibauchi, J. Wosnitza, N. E. Hussey, and Y. Matsuda, Phys. Rev. Lett. **124**, 107001 (2020).

[22] S. Kasahara, H. Suzuki, T. Machida, Y. Sato, Y. Ukai, H. Murayama, S. Suetsugu, Y. Kasahara, T. Shibauchi, T. Hanaguri, and Y. Matsuda, Phys. Rev. Lett. **127**, 257001 (2021).

[23] S. Kitagawa, G. Nakamine, K. Ishida, H. S. Jeevan, C. Geibel, and F. Steglich, Phys. Rev. Lett. **121**, 157004 (2018).

[24] C.-W. Cho, J. H. Yang, N. F. Q. Yuan, J. Shen, T. Wolf, and R. Lortz, Phys. Rev. Lett. **119**, 217002 (2017).

[25] S.-Z. Lin, D. Y. Kim, E. D. Bauer, F. Ronning, J. D. Thompson, and R. Movshovich, Phys. Rev. Lett. **124**, 217001 (2020).

[26] C.-w. Cho, J. Lyu, C. Y. Ng, J. J. He, K. T. Lo, D. Chareev, T. A. Abdel-Baset, M. Abdel-Hafiez, and R. Lortz, Nat. Commun. **12**, 2703 (2021).

[27] A. Devarakonda, T. Suzuki, S. Fang, J. Zhu, D. Graf, M. Kriener, L. Fu, E. Kaxiras, and J. G. Checkelsky, Nature (London) **599**, 51 (2021).

[28] K. Kinjo, M. Manago, S. Kitagawa, Z. Q. Mao, S. Yonezawa, Y. Maeno, and K. Ishida, Science **376**, 397 (2022).

[29] G. Koutroulakis, H. Kühne, H. H. Wang, J. A. Schlueter, J. Wosnitza, and S. E. Brown, arXiv:1601.06107.

[30] S. M. De Soto, C. P. Slichter, A. M. Kini, H. H. Wang, U. Geiser, and J. M. Williams, Phys. Rev. B **52**, 10364 (1995).

[31] Here, $D_{n,i}$ can be approximated as the internuclear dipole interaction d_{DI}, determined from the high-temperature spectra. The intensities of a doublet are $I_i = 1 \pm \sin(2\theta)$, with $\tan(2\theta) = d_{DI}/\delta K_m$, where δK_m is the difference between the doublet-averaged shifts of a given quartet.

[32] H. Shimahara and D. Rainer, J. Phys. Soc. Jpn. **66**, 3591 (1997).

[33] L. Bulaevskii, Zh. Eksp. Teor. Fiz. **65**, 1278 (1973).

[34] A. I. Buzdin and J. P. Brison, Europhys. Lett. **35**, 707 (1996).

[35] M. Houzet and A. Buzdin, Europhys. Lett. **50**, 375 (2000).

[36] J. Wosnitza, Ann. Phys. **530**, 1700282 (2018).

[37] By symmetry, the lowest-order coupling of the modulated part of the field-induced spin density scales with the square of the sinusoidally varying gap function. Consequently, the mean-field temperature variation of the modulated spin polarization would be $[T_c - T]^{2\beta}$, with $\beta = 1/2$. See Ref. [38].

[38] K. Machida and H. Nakanishi, Phys. Rev. B **30**, 122 (1984).